Static Slip Model of the 2017 M_w 5.4 Pohang, South Korea, Earthquake Constrained by the InSAR Data

by Seok Goo Song and Hoonyol Lee

ABSTRACT

An M_w 5.4 earthquake occurred in the city of Pohang in the southeastern part of the Korean Peninsula on 15 November 2017. It was a moderate-sized crustal event but triggered enormous attention from the Korean public because strong shaking was felt over the whole country, and it had been just a year since the M_w 5.5 Gyeongju earthquake, the largest instrumentally recorded event in the country. Both earthquakes occurred within 40 km of each other. The Pohang earthquake provides a unique opportunity to constrain the static slip model of an earthquake in Korea using spaceborne Interferometric Synthetic Aperture Radar (InSAR) observations because the focal depth is relatively shallow (~4 km), and surface displacement fields were successfully obtained by both descending and ascending orbits of the Sentinel-1A/B satellites. We performed a linear slip inversion using the InSAR data. Our slip model reveals that a major slip associated with the event occurred in the northeastern part of the hypocenter rather than in the southwestern part. In addition, its rupture dimension and mean slip are 5 km (width) by 6 km (length) and 15 cm, respectively. The InSAR data also show that no significant postseismic deformation occurred after the event.

Electronic Supplement: Tables of the estimated slip models.

INTRODUCTION

The Korean peninsula lies in the continental margin of the east Eurasian plate and as such is a moderately active seismic zone with ~10 $M > 3$ earthquakes occurring each year (Korea Meteorological Administration). A moderate-sized M_w 5.4 earthquake occurred in the city of Pohang in the southeastern part of the Korean Peninsula on 15 November 2017 (Fig. 1). It was a moderate-sized inland crustal event, but strong shaking was felt across the whole country, alarming many people because it had been just a year since the M_w 5.5 Gyeongju earthquake, the largest instrumentally recorded event on the Korean Peninsula (Lee and Song, 2016). The Gyeongju earthquake occurred close to the Pohang location (~40 km to the south). The moment tensor inversion results show that it was an oblique thrust event at a relatively shallow depth (~4 km; Cho, 2018). The locations of aftershocks also confirmed the geometry of the responsible fault plane. The M_w 5.4 Pohang earthquake was slightly smaller than the M_w 5.5 Gyeongju earthquake, but the focal depth was relatively shallow (~4 km). Sedimentary basin effects near the epicenter caused more damage than expected for an earthquake of this size (J.-H. Choi *et al.*, unpublished manuscript, 2018, see Data and Resources).

In the aftermath of the 2016 Gyeongju and 2017 Pohang earthquakes, the seismic hazard of southeast Korea has been brought to attention. Lee and Yang (2006) showed that there were many destructive events ($M > 6$) recorded in historical documents in the region. There are several geologically recognized fault lines, as shown in Figure 1. The longest fault line is approximately 170 km long and is called the Yangsan fault. Lee and Na (1983) first investigated microseismic activities around this fault and claimed that the Yangsan fault may still be seismically active. Kyung, Lee, and Okada (1999) and Kyung, Lee, Okada, *et al.* (1999) also found Quaternary displacements in paleoseismological studies, which included trench surveys. It is important to understand the physical properties of the Gyeongju and Pohang earthquakes to investigate the seismic hazards in the region.

In this study, we constrained the coseismic static slip distribution on the fault plane that was caused by the Pohang earthquake by inverting ground surface displacement data that were obtained by processing Sentinel-1A/B Interferometric Synthetic Aperture Radar (InSAR) observations. Both descending and ascending orbits were considered in the inversion. The Pohang earthquake provides a unique opportunity to constrain the static slip model using surface InSAR observations because the focal depth is relatively shallow (~4 km) and significant surface displacement fields were observed above the error range of the InSAR data. To our knowledge, this is the first study to constrain a nonuniform coseismic slip distribution of an earthquake by inverting InSAR data from the Korean Peninsula.

 doi: 10.1785/0220180156

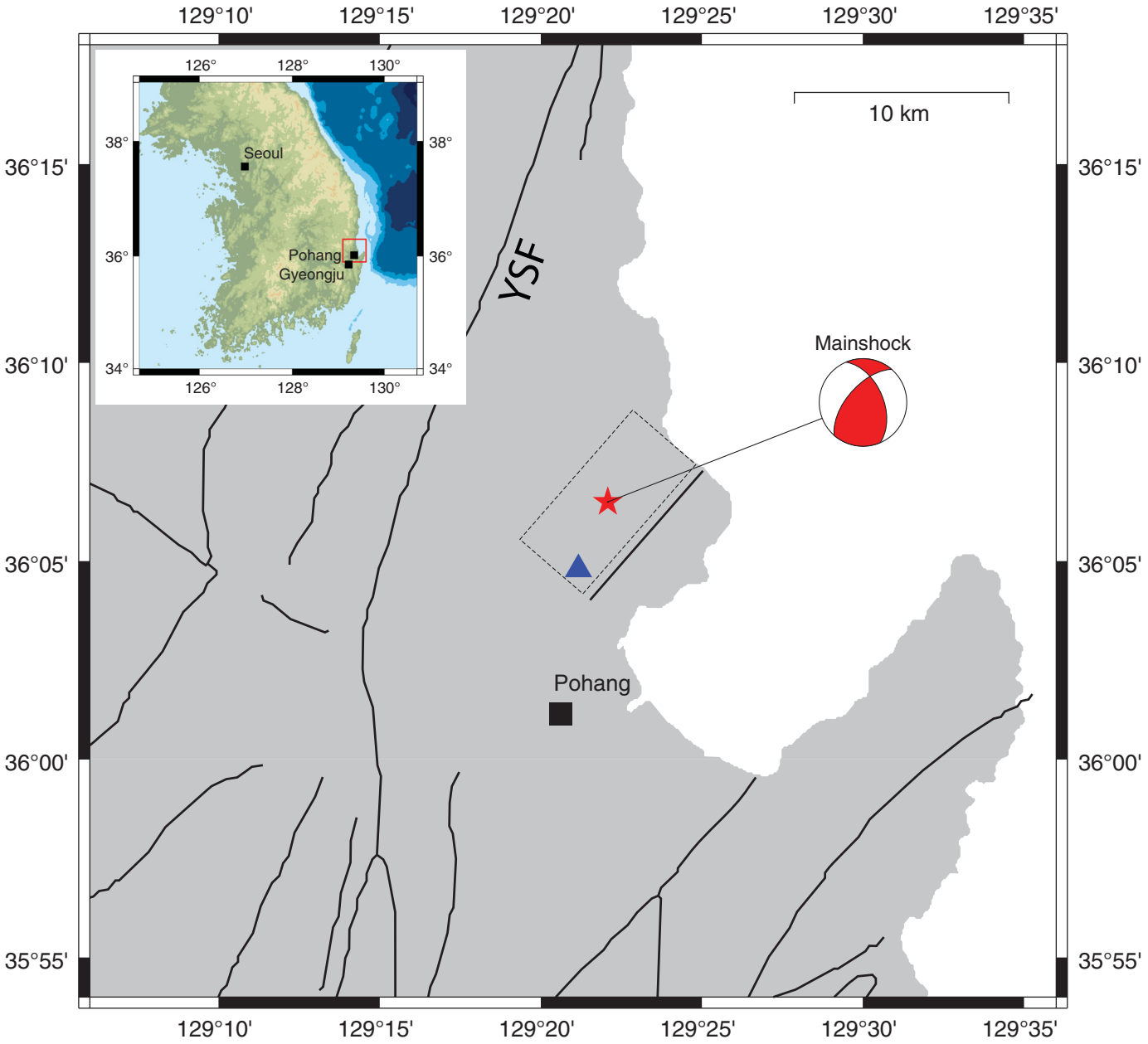

▲ **Figure 1.** The location of the Pohang earthquake and the geometry of the faulting plane. (Inset) The plotting area is indicated with a red box. The dashed rectangle is the surface projection of the imposed fault plane, and the solid line is the location of the fault trace on the surface assuming that the fault is extended to the surface with the same dip angle. The epicenter (red star) is plotted with the source mechanism (pure double component only) of oblique thrust faulting, which is adapted from Cho (2018). The location of one Global Navigation Satellite Systems (GNSS) station operated by Korea Institute of Geosciences and Mineral Resources is indicated by a blue triangle (Ji *et al.*, 2018). The surface traces of the faults in the region, obtained by geological surveys, are also presented (Chwae *et al.*, 1995). The Yangsan fault (YSF) is located in the northwest of the event.

DATA

InSAR has been widely used to detect surface coseismic displacement with centimeter-scale accuracy. Although atmospheric phase delays may add error on the scale of a few centimeters, the InSAR coseismic signal can easily be identified when the signal is strong and localized. Sentinel-1A/B satellites are equipped with a C-band Synthetic Aperture Radar (SAR) sensor in 12-day revisit cycle, 6 days apart from one another. The main observation mode is interferometric wideswath, which provides a 250-km swath for the global InSAR mapping strategy. Such a global mapping scheme enables a 12-day or even 6-day revisit cycle of an InSAR pair with a small baseline component perpendicular to the radar line of sight, thus providing an interferogram with high coherence. Other operating satellites such as TerraSAR-X, COSMO-SkyMed, and Radarsat-2 did not cover the

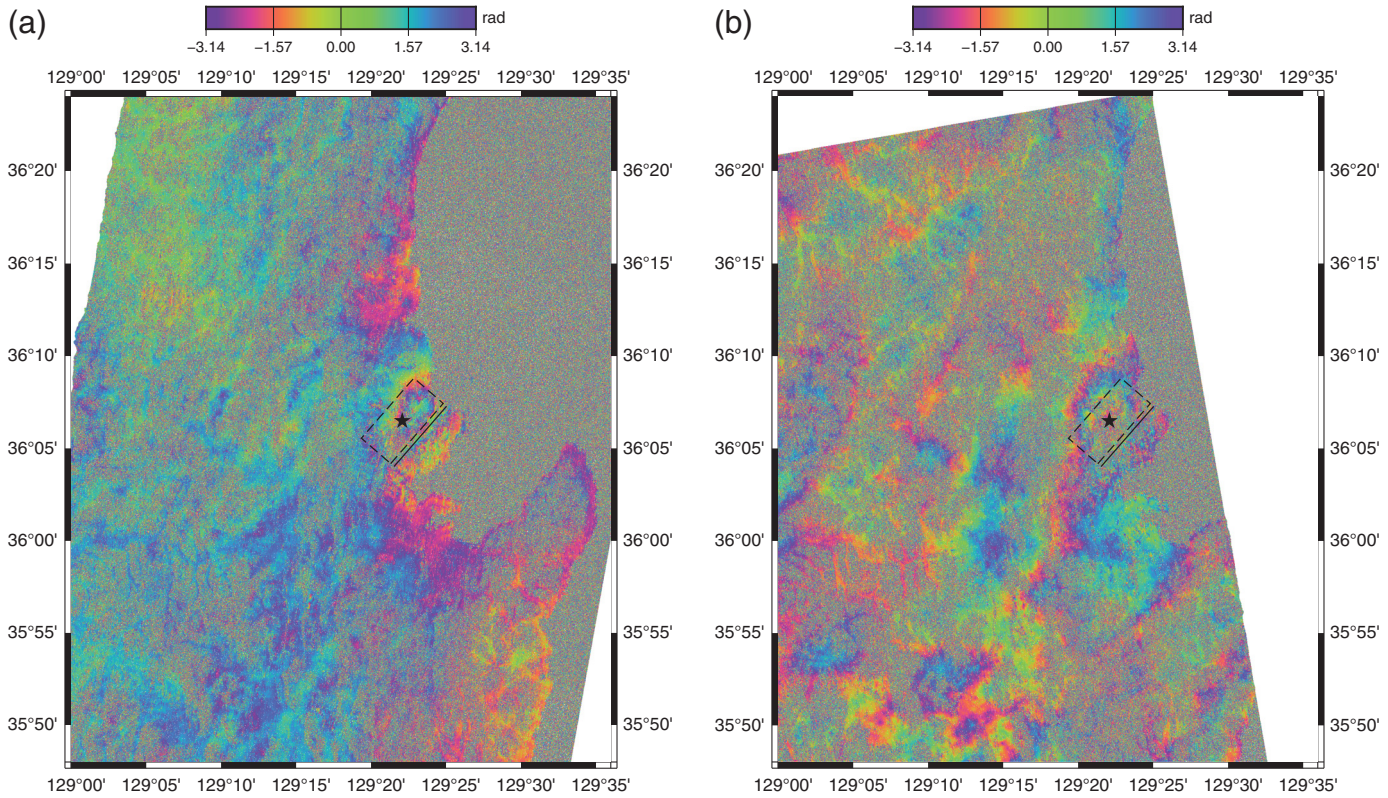

▲ **Figure 2.** Differential Interferometric Synthetic Aperture Radar (DInSAR) interferogram. (a) Descending, (b) ascending. Atmospheric and soil moisture errors are more significant on the ascending image because of precipitation. The location of the epicenter (star) and the geometry of the faulting plane are shown, equivalent to the ones in Figure 1.

study area in a routine basis, and the coseismic InSAR pair with a short temporal baseline is very rare for such an unexpected event. The spatial baseline is sometimes too large, beyond the critical value, and therefore it is difficult to maintain the orbital tube even in the case of emergency observations when the orbit is not designed for interferometric purposes (e.g., KOrea Multi-Purpose SATellite-5 [KOMPSAT-5]). The observation mode of other satellites (e.g., Advanced Land Observing Satellite-2 [ALOS-2]) changes frequently, disabling InSAR formation. Even L-band onboard ALOS-2 satellite can hardly maintain coherence because of changes in vegetation such as those associated with agricultural activities. Therefore, a regular observation scheme imposed on Sentinel-1A/B is crucial to the reliable InSAR observation of unpredictable earthquakes. InSAR measures the radar line-of-sight (LOS) component of surface displacement. It would be ideal to observe InSAR data from three preferably orthogonal LOS directions to measure a surface displacement vector. Sentinel-1A/B satellites provide two different LOSs from descending and ascending orbits, enabling reliable displacement components in the east–west and the up–down directions.

For the Pohang coseismic data, we used two Sentinel-1A/B–InSAR pairs, one in descending orbit and the other in ascending orbit. The descending, right-looking InSAR pair was obtained by Sentinel-1B on 4 and 16 November 2017. The ascending pair was obtained by Sentinel-1A on 10 November and 4 December 2017. Data processing was performed with the Sentinel Application Platform (SNAP) software that is provided freely by the European Space Agency (see Data and Resources). First accurate orbit data were implemented followed by coregistration of two SAR images. The flat-earth phase and topographic phase were removed using precise orbit data and Shutter Radar Topography Mission 1 arcsec data (Jarvis *et al.*, 2008). The resulting differential InSAR (DInSAR) images are shown in Figure 2a for the descending pair and Figure 2b for the ascending pair. Phase unwrapping was performed using the snaphu program (see Data and Resources), after which zero displacement was determined statistically. The resulting LOS displacements are shown in Figure 3a for the descending pair and Figure 3b for the ascending pair. The event occurred in a relatively high-coherence season of the year after harvest on a dry rice paddy, with fallen leaves and fire-damaged sparse vegetation in the mountains. The epicenter was on a dry rice paddy and the uplift and easting signal occurred mostly over the fire-damaged mountains along the coast. Other mountains are mostly covered with dense pine trees and have very low coherence. Urban areas maintain high coherence as well.

METHOD

InSAR data have often been used to constrain the coseismic slip distribution of crustal earthquakes (Hernandez *et al.*, 1999;

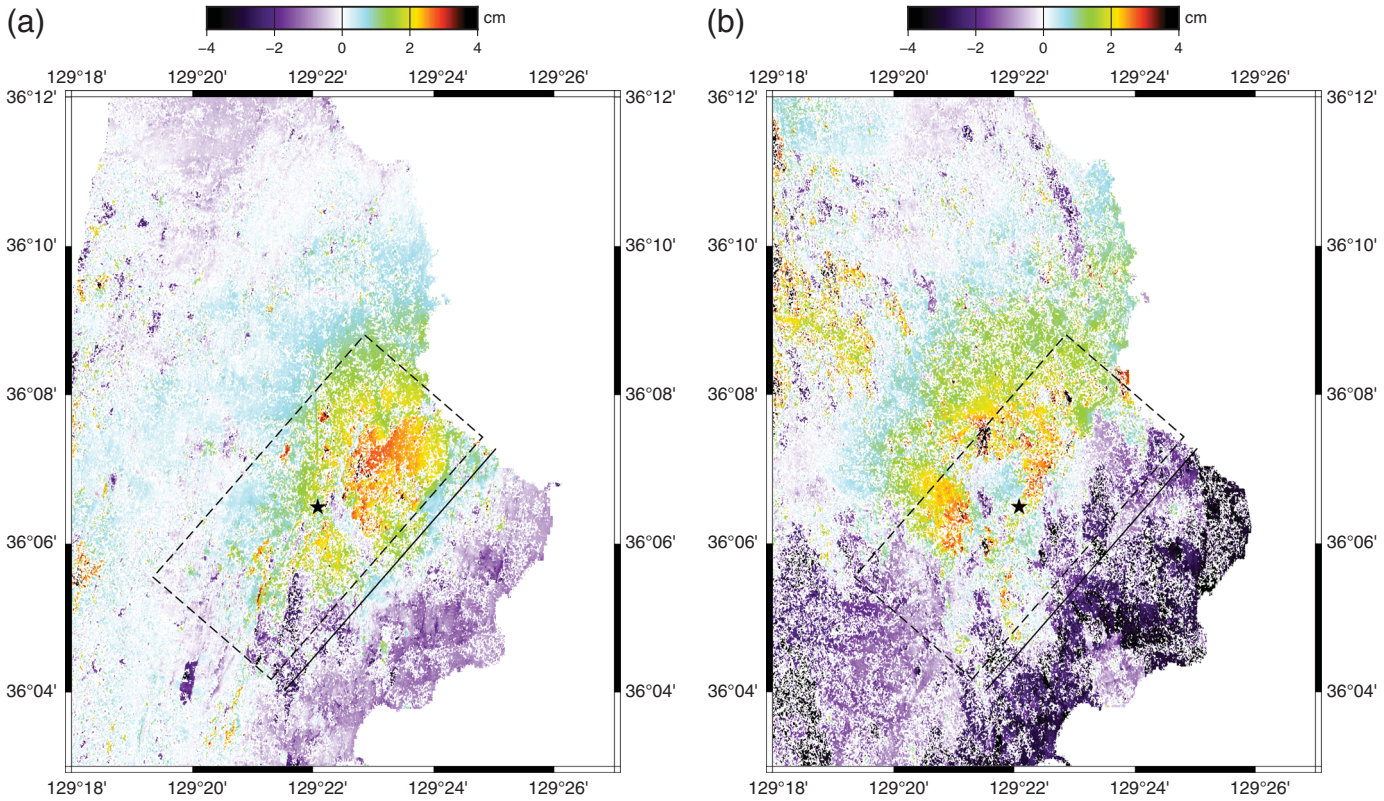

▲ **Figure 3.** Ground surface displacement fields obtained from Interferometric Synthetic Aperture Radar (InSAR) data. (a) Sentinel-1B DInSAR image in descending, right-looking mode. Positive values indicate uprising and easting coseismic displacements, whereas negatives are subsidence and westing. (b) Sentinel-1A DInSAR image in ascending, right-looking mode. Whereas positive values indicate uprising and westing coseismic displacements, negatives are subsidence and easting. Displacements with coherence values greater than 0.3 are displayed in (a,b). The location of the epicenter (star) and the geometry of the faulting plane are shown, equivalent to the ones in Figure 1.

Delouis *et al.*, 2002; Jonsson *et al.*, 2002). We performed a linear slip inversion using the two-component displacement fields obtained from the InSAR data. The ground displacement fields caused by the Pohang event were obtained in two LOS directions, that is, both descending and ascending (Table 1). The location and geometry information of the fault plane was obtained in a previous study (Cho, 2018), as summarized in Table 2. The length and width of the rupture dimension were set as 8 km long and 8 km wide, respectively. The width was set to be larger than the estimate from the aftershocks' distribution in order not to exclude possible slip, especially near the surface. Given a unit amount of slip on the fault plane, ground displacement fields were computed using the Okada (1985) method, assuming a homogeneous half-space. Each fault patch has dimensions of 0.5 km by 0.5 km. The patch size was determined to make it small enough to show the spatial variation of the fault slip, but it may not necessarily represent the level of the true resolution of slip estimates because the model space was regularized in the inversion. If the rake angle is fixed, based on the moment tensor solution, there are 192 model parameters in the inversion to represent the distribution of static slip for each subfault patch. The nonnegative least-squares approach was applied to invert the processed ground displacement fields with minimum norm regularization, as shown in the following equation:

Table 1
Information about the Sentinel-1A/B Interferometric Synthetic Aperture Radar (InSAR) Datasets

	Temporal Baseline	Line of Sight
Descending	12 days (4–16 November)	(0.6329, −0.1126, 0.7660)
Ascending	24 days (10 November–4 December)	(−0.6391, −0.1481, 0.7547)

Table 2
Fault Geometry

Length and width	(8 km, 8 km)
Epicenter	(129.3680°, 36.1082°)
Focal depth	4.3 km
Strike, dip, rake	(221°, 61°, 134°)

$$\begin{pmatrix} \mathbf{G} \\ \alpha^2\mathbf{I} \end{pmatrix}\mathbf{m} = \begin{pmatrix} \mathbf{d} \\ 0 \end{pmatrix}, \quad (1)$$

in which **m** and **d** are model and data vectors, respectively. **G** is the forward operator to link the slip on the fault to the ground displacement in the direction of LOS. To construct the matrix **G**, we first computed three-component Green's function matrix as defined by the Okada method. Then it was converted into the LOS angles of the satellite (Table 1). **I** is the identity matrix, and α^2 determines the relative level of regularization in the inversion, which is determined by the L-curve (Aster *et al.*, 2005). The data vector **d** is composed of ground-motion displacements in the two LOS directions. The data field is a 10 km by 10 km square box, centered at the epicenter. The interval of the data points was downsampled approximately 10 times from the original data and 0.11 and 0.14 km in the east–west and north–south directions, respectively. Displacement values with coherence greater than 0.3 were used in the inversion, which are approximately 57% and 37% of the initial descending and ascending orbit data points, respectively. Two versions of slip models were obtained by inverting the data from the descending orbit only and both the descending and ascending orbits.

RESULTS

Figure 4 shows the estimated slip distributions on the fault plane that were obtained by inverting the descending orbit data only and both the descending and ascending orbit data. The appropriate regularization levels were determined by the L-curve approach, as shown in Figure 5. Both slip models reveal that a major slip of the event occurred in the northeastern part of the hypocenter. However, the slip distributions obtained by both orbits show slip asperity at the deeper parts close to the hypocenter (Fig. 4b). Whereas the time span of the ascending orbit is 24 days, that of the descending orbit is 12 days (Table 1). Additionally, it snowed in the region on 24 November. We expect that the quality of the ascending orbit data may be degraded slightly because of this. Because both orbits provide constraints from two look directions, we consider the model that was obtained by the data from both orbits to be more reliable. The significant rupture dimensions and its mean slip are 6 km (length) by 5 km (width) and 15 cm, respectively. The moment magnitude estimates (M_w) computed by both slip models in Figure 4 are 5.4, which is consistent with that computed using the moment tensor inversion with the regional seismic data (Cho, 2018).

Figures 6 and 7 show the ground surface displacement data fitting in the LOS directions using the estimated slip models in Figure 4a and 4b, respectively. The data fitting can be quantified with variance reduction (VR), as defined in the following equation:

$$\mathrm{VR} = \left(1 - \frac{\|\mathbf{d}^{\mathrm{obs}} - \mathbf{d}^{\mathrm{pre}}\|_2^2}{\|\mathbf{d}^{\mathrm{obs}}\|_2^2}\right) \times 100, \quad (2)$$

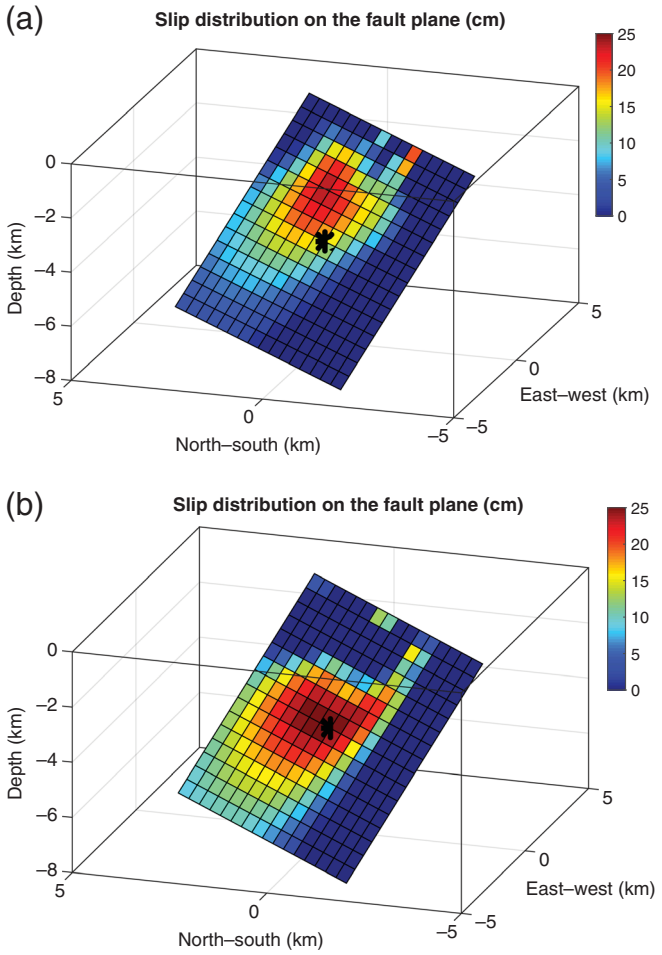

▲ **Figure 4.** Estimated static slip distributions. (a) The slip model was obtained from the descending orbit data only, and (b) the slip model was obtained from both the descending and ascending orbit data.

in which $\mathbf{d}^{\mathrm{obs}}$ and $\mathbf{d}^{\mathrm{pre}}$ are observed and predicted data vectors, respectively. The VR in Figure 6 is 61% and 52% in Figure 7. The data misfit was slightly degraded when we inverted the

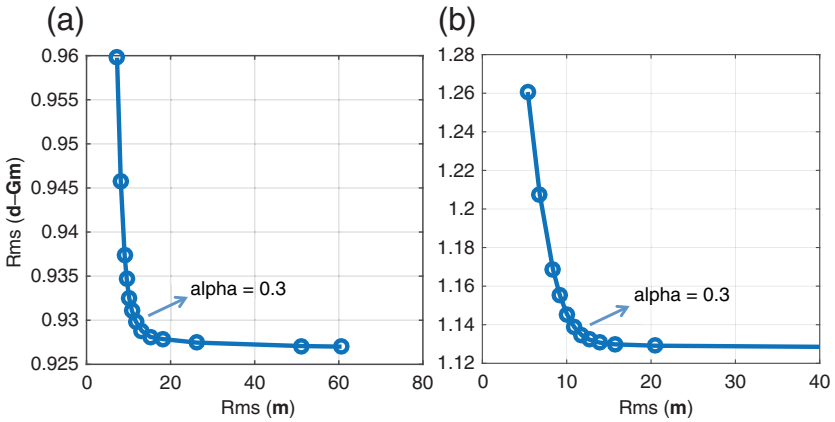

▲ **Figure 5.** L-curve. (a) Descending orbit data only and (b) both descending and ascending orbit data.

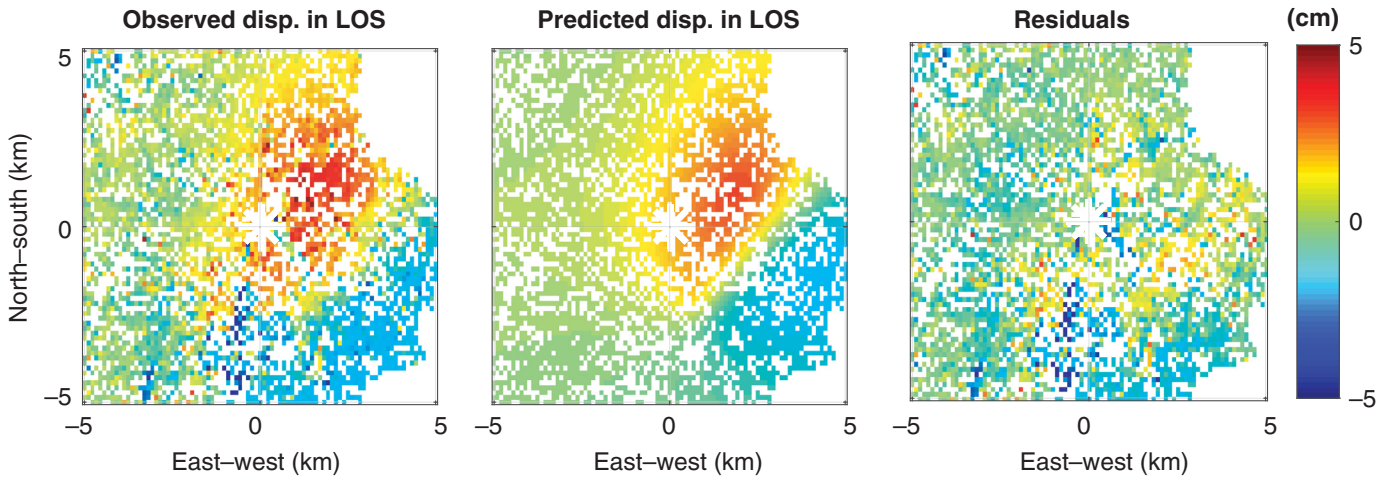

▲ **Figure 6.** Ground surface displacement data fitting in the line-of-sight (LOS) direction of the descending orbit using the estimated slip model in Figure 4a. Displacement values not used in the inversion because of its small coherence (< 0.3) are indicated in white.

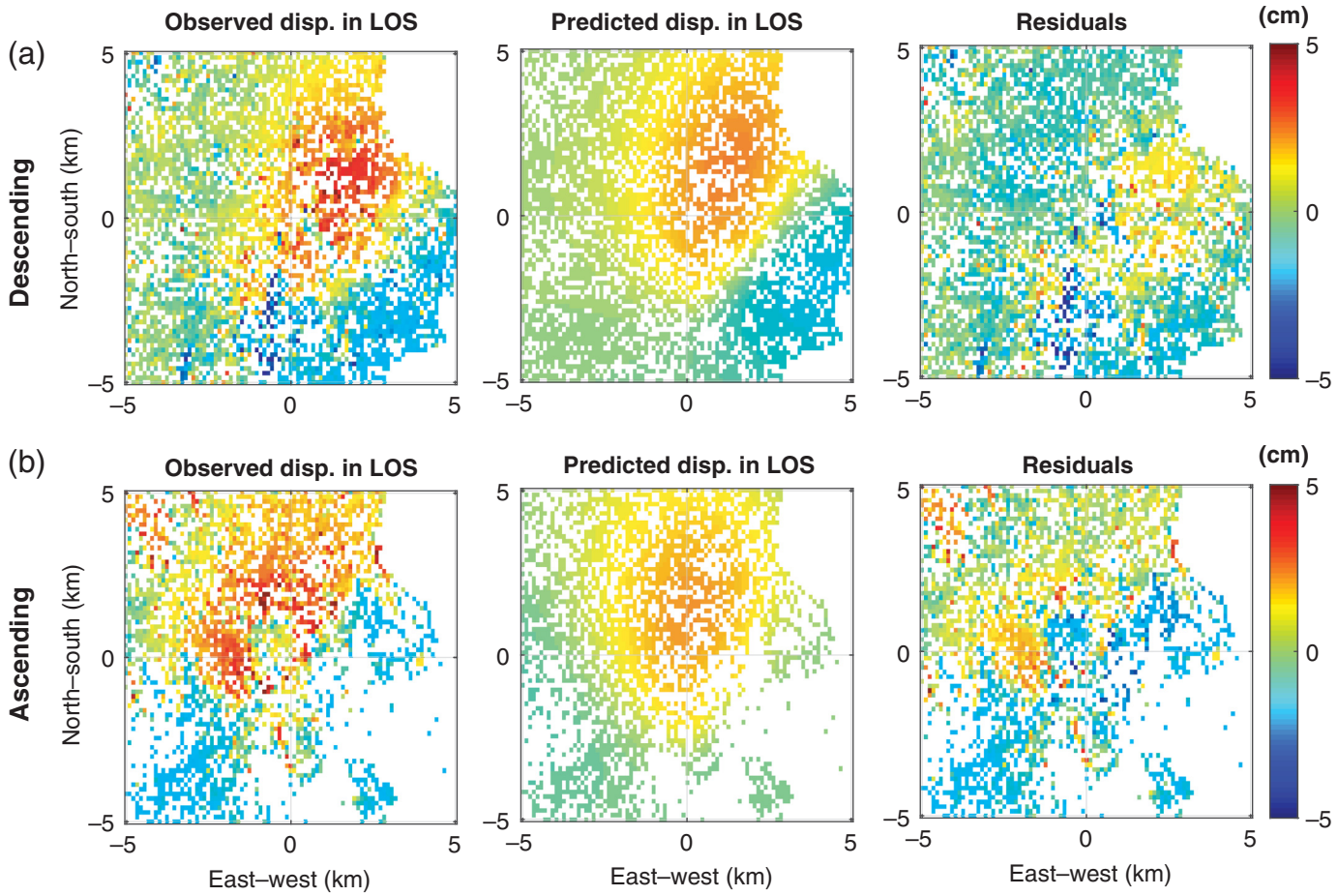

▲ **Figure 7.** Ground surface displacement data fitting in the LOS directions of both the (a) descending and (b) ascending orbits using the estimated slip model in Figure 4b. Displacement values not used in the inversion because of its small coherence (< 0.3) are indicated in white.

data from both orbits, and the misfit was more significant in the ascending orbit (Fig. 7b). However, we consider the second model to be more reliable because more independent data were included in the inversion.

Although the data fitting was performed in both LOS directions, it is useful to compute the three-component orthogonal displacement fields, as shown in Figure 8. This information was also useful when field geologists surveyed the region near

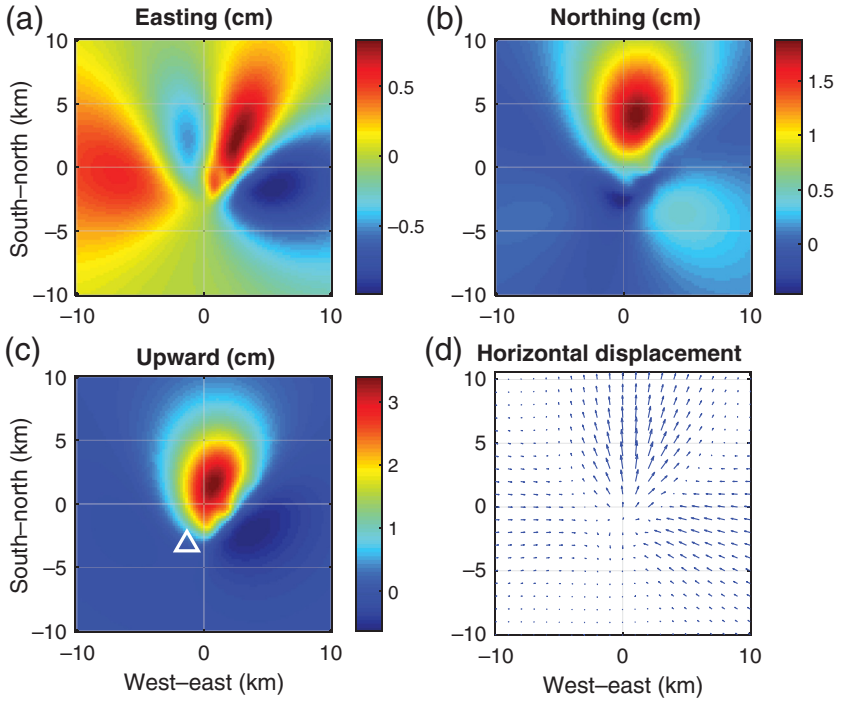

▲ **Figure 8.** Predicted ground surface displacement fields computed by the slip model in Figure 4b. (a) East–west component, (b) north–south component, (c) up–down component, and (d) horizontal displacement fields. The location of the GNSS station is indicated by the white triangle in (c).

the epicenter immediately after an earthquake occurred (J. H. Choi, personal comm., 2018). We observed that the maximum upward motion is greater than 3 cm. It is also interesting to note that the horizontal displacement fields are oriented toward the north above the slip asperity. Because the event has oblique slip (rake: 134°) on the dipping fault plane (dip: 61°), it is difficult to predict the direction of ground surface displacement by insight. One Global Navigation Satellite Systems (GNSS) station was being operated during the event, as shown in Figure 1. It is located in the southern edge of the prescribed fault plane, although significant fault slip was not observed in this region (Fig. 4). Ji *et al.* (2018) observed approximately 1-cm upward motion in this station during the event. Our predicted vertical motion in this location, as shown in Figure 8c, is near zero or slightly above zero (~0.1 cm). The GNSS data can provide additional independent geodetic constraint, and our model prediction does not seem to be significantly inconsistent with the GNSS observation. The InSAR data also show that no significant postseismic deformation was present after the event (Fig. 9). This is also confirmed by the fact that the moment magnitude estimate, constrained by the InSAR data, is consistent with the estimate from seismic data.

DISCUSSION

The Pohang earthquake was nucleated at a depth of ~4 km, which is relatively shallow for inland crustal events in the Korean Peninsula, especially considering its size. However, its shallow depth provides a unique opportunity to constrain the coseismic static slip distribution of the event using satellite InSAR data. It is also helpful that the event occurred in early winter after harvesting. Most seismic events in the country have been studied by investigating recorded seismic waveforms, but this event clearly demonstrates that geodetic data, including both InSAR and GNSS data, can contribute to constraining the earthquake source as long as significant ground surface deformation is detected.

It was fortunate to obtain relatively reliable ground surface deformation data for the Pohang earthquake by processing the InSAR data. However, atmospheric and soil moisture errors and time span should play an important role in determining the accuracy of the surface displacement estimates. Statistical analysis of the DInSAR interferogram of the descending and the ascending pairs shows that the fringe lengths—the length for one cycle (2.8 cm LOS displacement) of atmospheric or soil moisture error—are greater than 100 and 20 km/cycle, respectively. However, the displacement signature near the epicenter is highly localized so that the fringe lengths of the displacement are 2.5 km/cycle for the descending and 5 km/cycle for the ascending. Considering the fringe length of the atmospheric/soil error, the overall error near the epicenter is estimated to be 0.14 cm for the descending pair and 0.7 cm for the ascending pair. Even though there is no way of removing such errors, we believe that the displacement signal over the epicenter from both the descending and ascending orbit data is distinct enough to be positively identified as earthquake displacement.

The moment tensor inversion of the event shows that it has relatively significant compensated linear vector dipole components rather than a pure double-couple mechanism (Cho, 2018; Song *et al.*, 2018). This may raise the possibility that the rupture process of the event might have been more complex than pure shear faulting on a single planar fault (Grigoli *et al.*, 2018; Kim *et al.*, 2018). The focal mechanisms of several major aftershocks of the event also show complex patterns, including both thrust and strike-slip motions (Cho, 2018). It is probable that the event might have occurred with more complex mechanisms, that is, variable slip directions with multiple fault planes. However, the primary goal of our study is to obtain a nonuniform slip distribution model on a single planar fault, assuming a best double-couple shear-faulting event. The complexity of the rupture process of the event may need to be investigated further in future studies.

Grigoli *et al.* (2018) determined the dimension (length and width) and geometry (strike, dip, and rake) of the faulting plane, assuming a uniform slip on a single planar fault, by fitting descending orbit InSAR data. Their estimate of dip angle

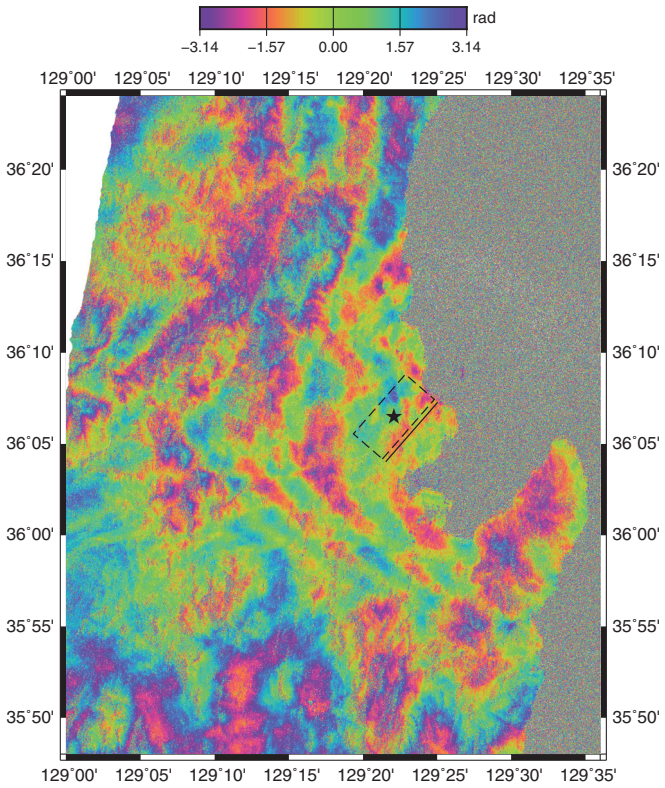

▲ **Figure 9.** Postseismic InSAR data (12 days; 16–28 November 2017). Most signals are presumably due to atmospheric and soil moisture changes. The location of the epicenter (star) and the geometry of the faulting plane are shown, equivalent to the ones in Figure 1.

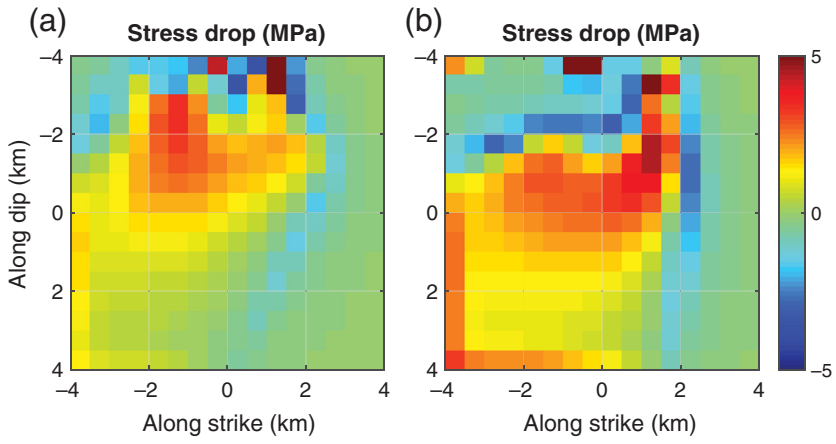

▲ **Figure 10.** Static stress-drop distributions computed by the static slip models in (a) Figure 4a and (b) Figure 4b, respectively. The stress drop was computed using the Okada (1992) method.

(75°) is much steeper compared with our input (61°) and the estimate (65°) obtained by the relocation of aftershocks using local temporary seismic stations (Kim *et al.*, 2018). Their estimate (~1.6 km) of the rupture width is narrower compared with our estimate (5 km), resulting in a large mean slip estimate (~1 m). The Pohang earthquake and its aftershocks were well recorded by both permanent and temporary seismic stations (Kim *et al.*, 2018). The hypocenter relocation of aftershocks, using the permanent and temporary seismic stations, should be able to provide accurate information about the fault geometry of the event. Thus, we think that it is meaningful to obtain a nonuniform slip model by fitting both descending and ascending orbit InSAR data, assuming the fault geometry obtained by the local seismic data. We also found that our model fits the data significantly better than the model suggested by Grigoli *et al.* (2018) if we include the ascending orbit data.

Uchide and Song (2018) showed that the static stress drop associated with the Gyeongju event is relatively large. The mean stress drop of the event is ~20 MPa. However, the mean stress drop of the Pohang event (Fig. 10) is apparently much smaller, that is, approximately 2 MPa. We think that this is partially because of the shallow focal depth of the event, including the free surface effect. In addition, the slip model was estimated by the static ground surface displacement fields, which might produce a smoother slip distribution on the model with oversmoothing. Two moderate-sized events, the 2016 Gyeongju and 2017 Pohang earthquakes, clearly indicate that seismic hazards in southeast Korea are not ignorable. An in-depth understanding of the source characteristics of the events should help investigate the seismic hazards in the region. In addition, we demonstrated that the satellite InSAR data are useful if significant ground surface deformation is detected.

CONCLUSION

The 2017 M_w 5.4 Pohang earthquake occurred in the southeast part of the Korean Peninsula and triggered tremendous concerns regarding seismic hazards in the country because the earthquake occurred only one year after the M_w 5.5 Gyeongju earthquake, the largest recorded event on the Peninsula, at a close location (~40 km away). The Pohang event occurred at a relatively shallow depth (~4 km) and produced a significant amount of ground surface deformation, which was well captured by InSAR data. We successfully modeled the coseismic static slip distribution of the event on the predescribed fault plane by inverting ground surface displacement data obtained by processing a Sentinel-1 InSAR image, which is the first attempt for the Korean Peninsula. A significant slip distribution is observed in the northeastern part of the hypocenter, and the rupture dimensions and its mean slip are 6 km (length) by 5 km (width) and 15 cm, respectively. The moment magnitude estimates (5.4) are consistent with that computed using regional seismic data. The InSAR data are useful in providing independent constraint to understand the characteristics of the earthquake source in

addition to seismic data as long as the ground surface deformation is well detected.

DATA AND RESOURCES

Sentinel-1A/B Synthetic Aperture Radar (SAR) data were obtained freely from the Copernicus Open Access Hub of European Space Agency (http://scihub.copernicus.eu, last accessed May 2018). The Sentinel Application Platform (SNAP) software was downloaded freely from the Science Toolbox Exploitation Platform (STEP; http://step.esa.int/main/toolboxes/snap, last accessed May 2018). The snaphu program was provided by the Stanford Radar Interferometry Research Group (https://web.stanford.edu/group/radar/softwareandlinks/sw/snaphu/, last accessed October 2018). The unpublished manuscript by J.-H. Choi *et al.*, "Surface deformations and rupture processes associated with the 2017 M_w 5.4 Pohang earthquake, Korea", submitted to *Bull. Seismol. Soc. Am.*

ACKNOWLEDGMENTS

The authors thank Associate Editor B. Crowell and two anonymous reviewers for their thoughtful comments, which improved our article significantly. The authors are indebted to C. S. Cho for providing his moment tensor inversion results. They also benefited from useful discussions with J. H. Park, C. S. Cho, J. H. Choi, and K. H. Ji throughout the study. This work was supported by the Basic Research Project of Korea Institute for Geosciences and Mineral Resources (KIGAM), funded by the Ministry of Science and ICT of Korea, and the National Research Foundation of Korea (NRF—2016R1D1A1A09916630). Some of the figures in the article were drawn using the Generic Mapping Tools (Wessel and Smith, 1991).

REFERENCES

Aster, R. C., B. Borchers, and C. H. Thurber (2005). *Parameter Estimation and Inverse Problems*, Elsevier Academic Press, San Diego, California.

Cho, C. S. (2018). Characteristics of Pohang earthquake (M_w 5.4) occurred near developing geothermal well and relative relocations of aftershocks using Hierarchical Clustering, *Annual Meeting of European Geoscience Union*, Vienna, Austria, 8–13 April 2018, EGU2018–6850.

Chwae, U. C., K. B. Kim, S. H. Hong, B. J. Lee, J. H. Hwang, K. H. Park, S. K. Hwang, P. Y. Choi, K. Y. Song, and M. S. Jin (1995). *Geological Map of Korea (Scale 1:1,000,000)*, Korea Institute of Geoscience and Mineral Resources, Daejeon, South Korea.

Delouis, B., D. Giardini, P. Lundgren, and J. Salichon (2002). Joint inversion of InSAR, GPS, Teleseismic, and strong-motion data for the spatial and temporal distribution of earthquake slip: Application to the 1999 Izmit mainshock, *Bull. Seismol. Soc. Am.* **92,** 278–299.

Grigoli, F., S. Cesca, A. P. Rinaldi, A. Maconi, J. A. Lopez-Comino, J. F. Clinton, R. Westaway, C. Cauzzi, T. Dahm, and S. Wiemer (2018). The November 2017 M_w 5.5 Pohang earthquake: A possible case of induced seismicity in South Korea, *Science* **360,** no. 6392, doi: 10.1126/science.aat2010.

Hernandez, B., F. Cotton, and M. Campillo (1999). Contribution of radar interferometry to a two-step inversion of the kinematic process of the 1992 Landers earthquake, *J. Geophys. Res.* **104,** 13,083–13,099.

Jarvis, A., H. I. Reuter, A. Nelson, and E. Guevara (2008). Hole-filled SRTM for the globe, version 4, *CGIAR-CSI SRTM 90m Database*, available at http://srtm.csi.cgiar.org (last accessed November 2018).

Ji, K. H., S. G. Song, and C. S. Cho (2018). Geodetic observations of surface deformation due to the 2017 M_w 5.4 Pohang earthquake, Korea, *Fall Meeting of American Geophysical Union (AGU)*, Washington, D.C, 10–14 December 2018.

Jonsson, S., H. Zebker, P. Segall, and F. Amelung (2002). Fault slip distribution of the 1999 M_w 7.1 Hector Mine, California, earthquake, estimated from satellite radar and GPS measurements, *Bull. Seismol. Soc. Am.* **92,** 1377–1389.

Kim, K.-H., J.-H. Ree, Y. Kim, S. Kim, S. Y. Kang, and W. Seo (2018). Assessing whether the 2017 M_w 5.4 Pohang earthquake in South Korea was an induced event, *Science* **360,** no. 6392, doi: 10.1126/science.aat6081.

Kyung, J. B., K. Lee, and A. Okada (1999). A paleoseismological study of the Yangsan fault—Analysis of deformed topography and trench survey, *J. Korea Geophys. Soc.* **2,** 155–168 (in Korean).

Kyung, J. B., K. Lee, A. Okada, M. Watanabe, Y. Suzuki, and K. Takemura (1999). Study of the fault characteristics by trench survey in the Sangchon-ri area in the southern part of the Yangsan fault, Southeastern Korea, *J. Korea Earth Sci. Soc.* **20,** 101–110 (in Korean).

Lee, K., and S. H. Na (1983). A study of microearthquake activity of the Yangsan fault, *J. Geophys. Soc. Korea* **19,** 127–135.

Lee, K., and S. G. Song (2016). A preliminary study on the Gyeongju earthquakes in September 2016, *J. Natl. Acad. Sci. Repub. Korea* **55,** 25–39.

Lee, K., and W.-S. Yang (2006). Historical seismicity of Korea, *Bull. Seismol. Soc. Am.* **96,** 846–855.

Okada, Y. (1985). Surface deformation due to shear and tensile faults in a half-space, *Bull. Seismol. Soc. Am.* **75,** 1135–1154.

Okada, Y. (1992). Internal deformation due to shear and tensile faults in a half-space, *Bull. Seismol. Soc. Am.* **82,** 1018–1040.

Song, J.-H., J.-U. Woo, J. Rhie, S. Kim, and T.-S. Kang (2018). Source analysis of November 15, 2017 Pohang earthquake sequences: The first non-double couple event reported in South Korea, *Annual Meeting of European Geoscience Union*, Vienna, Austria, 8–13 April 2018, EGU2018–12279.

Uchide, T., and S. G. Song (2018). Fault rupture model of the 2016 Gyeongju, South Korea, earthquake and its implication for the underground fault system, *Geophys. Res. Lett.* **45,** 2257–2264.

Wessel, P., and W. H. F. Smith (1991). Free software helps map and display data, *Eos Trans. AGU* **72,** 441.

Seok Goo Song
Earthquake Research Center
Korea Institute of Geoscience and Mineral Resources
124 Gwahang-no, Yuseong-gu
Daejeon 34132
Republic of Korea
sgsong@kigam.re.kr

Hoonyol Lee
Department of Geophysics
Kangwon National University
1 Gangwondaehak-gil, Chuncheon
Gangwon-do 24341
Republic of Korea
hoonyol@kangwon.ac.kr

Published Online 21 November 2018